
DEEP LEARNING FOR BLIND SPECTRAL UNMIXING OF LULC CLASSES WITH MODIS MULTISPECTRAL TIME SERIES AND ANCILLARY DATA

A PREPRINT

José Rodríguez-Ortega

Dept. of Computer Science and Artificial Intelligence, DaSCI
University of Granada
Granada
e.jrodriguez98@go.ugr.es
LifeWatch-ERIC ICT Core
Seville
jose.rodriguez@lifewatch.eu

Rohaifa Khaldi

LifeWatch-ERIC ICT Core
Seville
rohaifa.khaldi@lifewatch.eu

Domingo Alcaraz-Segura

Dept. of Botany
Faculty of Science, University of Granada
Granada
dalcaraz@ugr.es

Siham Tabik

Dept. of Computer Science and Artificial Intelligence, DaSCI
University of Granada
Granada
siham@ugr.es

November 6, 2023

ABSTRACT

Remotely sensed data are dominated by mixed Land Use and Land Cover (LULC) types. Spectral unmixing is a technique to extract information from mixed pixels into their constituent LULC types and corresponding abundance fractions. Traditionally, solving this task has relied on either classical methods that require prior knowledge of endmembers or machine learning methods that avoid explicit endmembers calculation, also known as blind spectral unmixing (BSU). Most BSU studies based on Deep Learning (DL) focus on one time-step hyperspectral or multispectral data. To our knowledge, here we provide the first study on BSU of LULC classes using MODIS multispectral time series, in presence of missing data, with end-to-end DL models. We further boost the performance of a Long-Short Term Memory (LSTM)-based model by incorporating geographic plus topographic (geo-topographic) and climatic ancillary information. Our experiments show that combining spectral-temporal input data together with geo-topographic and climatic information substantially improves the abundance estimation of LULC classes in mixed pixels. To carry out this study, we built a new labeled dataset of the region of Andalusia (Spain) with monthly multispectral time series of pixels for the year 2013 from MODIS at 460m resolution, for two hierarchical levels of LULC classes, named Andalusia MultiSpectral MultiTemporal Unmixing (Andalusia-MSMTU). This dataset provides, at the pixel level, a multispectral time series plus ancillary information annotated with the abundance of each LULC class inside each pixel. The dataset ¹ and code ² are available to the public.

Keywords Land Use Land Cover (LULC) · Deep Learning · Spectral unmixing · Ancillary data · Missing values

¹<https://zenodo.org/record/7752348#.ZBmkkezMLdo>

²<https://github.com/jrodriguezortega/MSMTU>

1 Introduction

LULC mapping is normally addressed by classifying each pixel in a satellite image into a LULC class. Frequently, the spatial resolution of an image and the thematic resolution of its LULC legend do not match, which leads to the mixed pixel problem, where pixels are not pure but contain several LULC classes. Accordingly, many methods have tried to estimate the relative abundances of each LULC class in a pixel from the combined spectral signature [1]. Such estimation of the spectrum and the abundance of the LULC classes present within each pixel is known as spectral unmixing and is one of the most challenging areas of research in Remote Sensing (RS) [2]. Various unmixing approaches, including linear and nonlinear methods, have been developed [3, 4]. Many of these approaches require the use of the pure spectral signature (the endmember) of each LULC class. However, the acquisition of endmembers might be hard in areas dominated by mixed pixels [5]. To overcome this limitation, several works have introduced the concept of BSU as an alternative approach to avoid the need to derive any endmember spectra or making any prior assumption about their mixing nature. The difference between BSU and traditional or conventional spectral unmixing methods is illustrated in Figure 1.

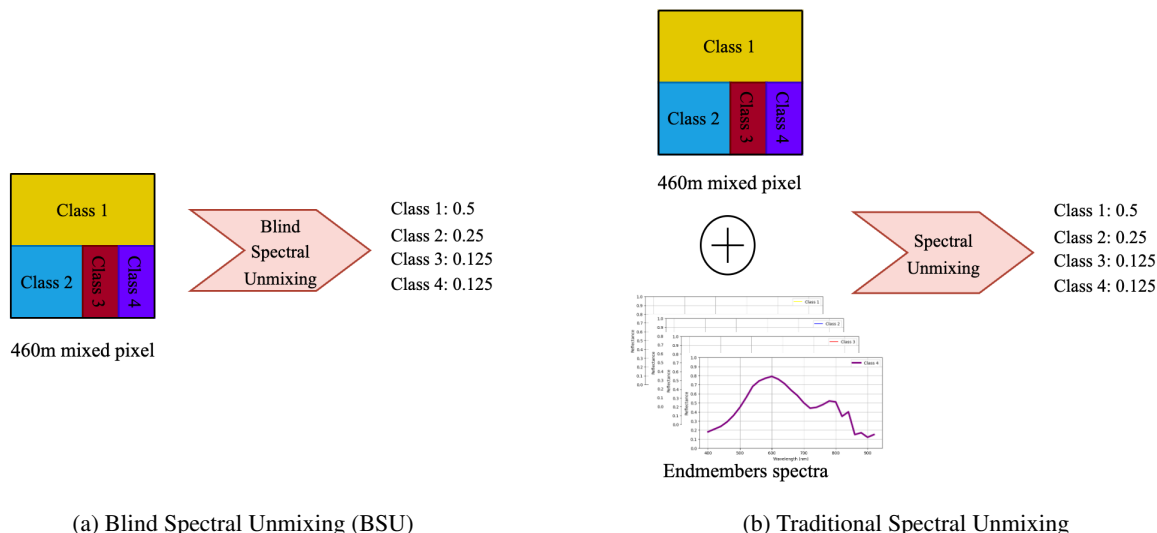


Figure 1: Toy example illustrating (a) Blind Spectral Unmixing (without endmember extraction) versus Traditional Spectral Unmixing (with endmember extraction) in a 460m mixed pixel.

In the last years, modern DL models have been increasingly employed for addressing BSU by directly learning the input-output mapping from the spectra of mixed pixels to their corresponding class abundances. Several studies explored the potential of DL methods for BSU in LULC mapping using either single time-step hyperspectral data [2, 6, 7] or single time-step multispectral data [8]. Including temporal information could be a great opportunity to improve BSU methods [4] and a few works (see Table 1) have started exploring approaches with multispectral time series data. However, to the best of our knowledge, none have explored an end-to-end DL solution, where recurrent neural networks (RNN) and particularly Long-Short Term Memory (LSTM) networks are a perfect fit.

In contrast to traditional methods, the application of DL in BSU facilitates the exploitation of ancillary information such as geographic location, topography, and climate. For example, in the field of computer vision, ancillary data has been successfully used by DL models to improve the performance during image classification [9, 10, 11]. However, the introduction of ancillary information remains unexplored in spectral unmixing methods. We hypothesize that injecting such ancillary information could boost the performance of the predictive model in spectral unmixing. This information may help the model understand the spatial distribution and variations in climate of the different LULC types.

Addressing spectral unmixing of LULC classes using multispectral time series data and ancillary information faces several challenges:

- Public labeled datasets with multispectral multitemporal data for spectral unmixing of LULC classes are not available.
- Creating a new dataset of multispectral time series plus ancillary information together with LULC abundances annotations is complex, costly and time consuming.

- Remote sensing data usually contains missing values due to atmospheric conditions or sensors’ errors, which requires applying robust processing techniques.
- Feeding ancillary information to spectral unmixing models is a promising direction but can be complex. Ensuring that these data improve the model robustness is a challenge and it is not explored yet.

To tackle the above mentioned challenges, we considered the longest-term time series with the highest frequency data provided by MODIS to create a regional-scale dataset of more than 500,000 MODIS 460m resolution pixels from Andalusia, Spain. This dataset provides, for each individual pixel, (1) a multispectral time series of monthly observations during the year 2013 of the seven spectral bands of the MODIS sensor, (2) ancillary information containing geographic, topographic and climatic variables, and (3) their corresponding LULC class abundances at two different levels of the classes hierarchy, extracted Andalusia’s official LULC map (SIPNA [12]). Furthermore, a first DL-based method is proposed for BSU, consisting of a two branch neural network (NN) where the first branch process the multispectral time series using a LSTM-based model capable of handling missing values, and the second branch process the ancillary information. A graphical illustration of the followed workflow in this study is shown in Figure 2.

The primary contributions of this research can be summarized as follows:

- Development of Andalusia-MSMTU dataset: a novel multispectral multitemporal labeled dataset with mixed pixels for Andalusia, a highly heterogeneous region in Spain. In addition to the multispectral multitemporal information, each mixed pixel has its corresponding geo-topographic and climatic information. Such dataset will open the possibility for new explorations.
- Design and analysis of a DL-based approach to estimate the abundance per pixel of LULC classes from multispectral time series data with and without ancillary information.

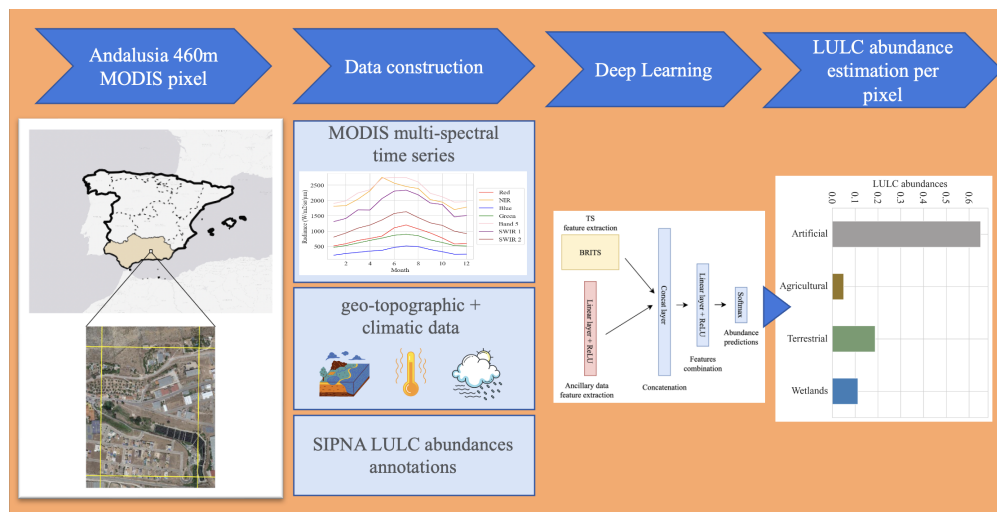


Figure 2: Flowchart of our proposed method. First, Andalusia-MSMTU dataset is built using MODIS multispectral multitemporal data plus geo-topographic and climatic data together with the corresponding LULC abundances annotations extracted from SIPNA. Subsequently, the deep learning based model is designed to use both, multi-spectral times series and geo-topographic and climatic data to estimate the LULC abundances.

The rest of this article is structured as follows: Section 2 presents the related work. Section 3 provides preliminaries and background. Section 4 introduces the study area and the data construction process. Section 5 describes the used DL methodology. Section 6 assesses the results obtained. Section 7 provides a comprehensive discussion of the results obtained, comparing them with previous works. Finally, section 8 concludes the findings and sheds light into future works.

2 Related work

The most related works to our multispectral multitemporal unmixing study are those that address the problem of spectral unmixing using DL based approaches and those that build labeled datasets especially designed for the unmixing problem.

2.1 Spectral unmixing using DL-based approaches

One of the first DL approaches for BSU was proposed by [13], where they introduced three spectral bands values and the neural network (NN) predicts the abundances of three LULC classes. [14] compared NN, Linear Mixture Models (LMM), and fuzzy c-means for spectral unmixing of LULC classes, being the NN the best model given sufficient training samples. Then, [15] proposed a two-stage NN architecture that first reduces the dimension of the input vector using an auto-associative NN, and performs abundance estimation out of the reduced input using a MLP. Recently, [6] evaluated autoencoders with different hyperparameters. [16] introduced MSNet, a multi-stage convolutional autoencoder network designed for hyperspectral linear unmixing, achieving this by capturing contextual relationships between pixels. Following the success of transformers architecture [17], [7] and [18] introduced NN architectures with the attention mechanism for abundance estimation.

Regarding RNN-based works, the only work on BSU using a LSTM-based network was introduced by [19]. They proposed a nonsymmetric autoencoder network with a LSTM component to capture spectral correlation together with an attention mechanism to further enhance the unmixing performance. For a more detailed review of DL methods in spectral unmixing see [20] and [4].

In parallel, there exist few works that incorporate ancillary data to improve the performance of DL models. Most of these studies occur in the field of computer vision, such as high inter-class similarity classification problems [9], plankton image classification [10] or crop type mapping [11].

Table 1: List of spectral unmixing works using multispectral and multitemporal data. HRM: Higher Resolution Map, PTU: Probabilistic Temporal Unmixing, FCLSU: Fully Constrained Least Squares Spectral Unmixing, TMA: Temporal Mixture Analysis, RF: Random Forest, OLS: Ordinary Least Square, STSU: Spatio-Temporal Spectral Unmixing, RSTSU: Real-time STSU, LSTM: Long-Short Term Memory.

Ref. & year	Study area	Source	Spatial-temporal res.	Annotations	# classes	Public	Approach
[21] 2004	Yaqui Valley (Mexico)	MODIS	500m - 8 obs. (months)	HRM (Landsat-derived)	3	No	PTU
	Great Plains (US)	MODIS	500m - 8 obs. (months)	HRM (Landsat-derived)	3	No	PTU
[22] 2011	The Netherlands	MERIS	300m - 7 obs. (months)	HRM (LGN5 L1)	4	No	FCLSU
	The Netherlands	MERIS	300m - 7 obs. (months)	HRM (LGN5 L2)	12	No	FCLSU
[23] 2012	Japan	MODIS	250m - 365 obs. (days)	HRM (Landsat-derived)	2	No	TMA-based
[24] 2020	Broome County (US)	Landsat	30m - (2000 to 2014)	HRM (NLCD)	2	No	RF
[25] 2020	Rondônia (Brazil)	Landsat	30m - (1990 to 2013)	HRM (Rondônia)	5	No	OLS + RF
[5] 2021	Daxing (China)	MODIS	480m - 3 obs. (months)	HRM (Landsat-derived)	2	No	STSU
	Zibo (China)	MODIS	480m - 3 obs. (months)	HRM (Landsat-derived)	2	No	STSU
	Amazon (Brazil)	MODIS	480m - 3 obs. (months)	HRM (Landsat-derived)	2	No	STSU
[26] 2021	Daxing (China)	MODIS	480m - 2 obs. (months)	HRM (Landsat-derived)	2	No	RSTSU
	Zibo (China)	MODIS	480m - 2 obs. (months)	HRM (Landsat-derived)	2	No	RSTSU
	Lichuan (China)	MODIS	480m - 2 obs. (months)	HRM (Landsat-derived)	2	No	RSTSU
Ours	Andalusia (Spain)	MODIS	460m - 12 obs. (months)	HRM (SIPNA L1)	4	Yes	LSTM-based
	Andalusia (Spain)	MODIS	460m - 12 obs. (months)	HRM (SIPNA L2)	10	Yes	LSTM-based

2.2 Labeled datasets based on LULC products

Supervised learning requires high amounts of ground truth data to achieve better generalization. One of the biggest limitations in spectral unmixing is the limited availability of ground truth LULC maps [4, 27]. Some areas or regions, especially in western countries, have LULC ground truth based on visual interpretation for specific fields of study. For example, SIPNA [12] was intended for territorial planning in Spain. Its annotation was carried out by experts during several years. This dataset can be used to annotate RS data.

In parallel, there exist several annotated multispectral multitemporal datasets prepared for supervised spectral unmixing (see Table 1). However, all of them are private.

Our work is the first in providing a public good quality multispectral multitemporal mixed pixel labeled dataset, named Andalusia-MSMTU, that includes not only spectro-temporal information but also geo-topographic and climatic ancillary data. Andalusia-MSMTU is organized into two hierarchical levels of classes with four and ten LULC types and it is especially suitable for building unmixing DL-based models for LULC abundance estimation.

3 Preliminaries and background

We define a multivariate time series as a sequence of observations $X = (\mathbf{x}_1, \mathbf{x}_2, \dots, \mathbf{x}_T)$, where T is the number of observations or time steps. Each observation $\mathbf{x}_t \in \mathbb{R}^C$ where $t \in \{1, \dots, T\}$ consists of C variables, such that $\mathbf{x}_t = \{x_t^1, x_t^2, \dots, x_t^C\}$.

3.1 Recurrent Neural Network

RNN [28] is a NN architecture specifically designed for handling sequential data. RNN consider the sequential relationship of inputs by using a shared function f to process each input. RNN process the time series using a recurrence approach at every time step t , computing a hidden state \mathbf{h}_t by considering the previous hidden state \mathbf{h}_{t-1} and the current input \mathbf{x}_t :

$$\mathbf{h}_t = f(\mathbf{h}_{t-1}, \mathbf{x}_t) \quad (1)$$

where \mathbf{h}_0 is normally, at the beginning, the zero vector, i.e., $\mathbf{h}_0 = \mathbf{0}$.

There are several choices on how to process sequential information. In this work, we focus on the LSTM network, which is an improvement of normal RNN solving some of its biggest limitations [29]

3.2 BRITS

In time series data and specifically in RS data, it is common to find missing values due to sensor errors, cloud cover and more [30]. To handle this situation, there exists a type of RNN architecture that can learn to solve two tasks simultaneously: imputing missing values and classifying the input sequence data. This model is called Recurrent Imputation for time series (RITS) [31]. The RITS model perform the imputation algorithm to assist the classification task and obtain the final classification as:

$$\hat{\mathbf{y}} = f_{out}(\mathbf{h}_T) \quad (2)$$

In practice, considering only unidirectional forward dynamic is problematic due to slow convergence, inefficiency in training and bias exploding problem [31]. To overcome these issues a bidirectional version named Bidirectional RITS (BRITS) model is proposed to learn forward and backward patterns by accessing information from past and future at any given time step. The final scheme of BRITS can be seen in Figure 3.

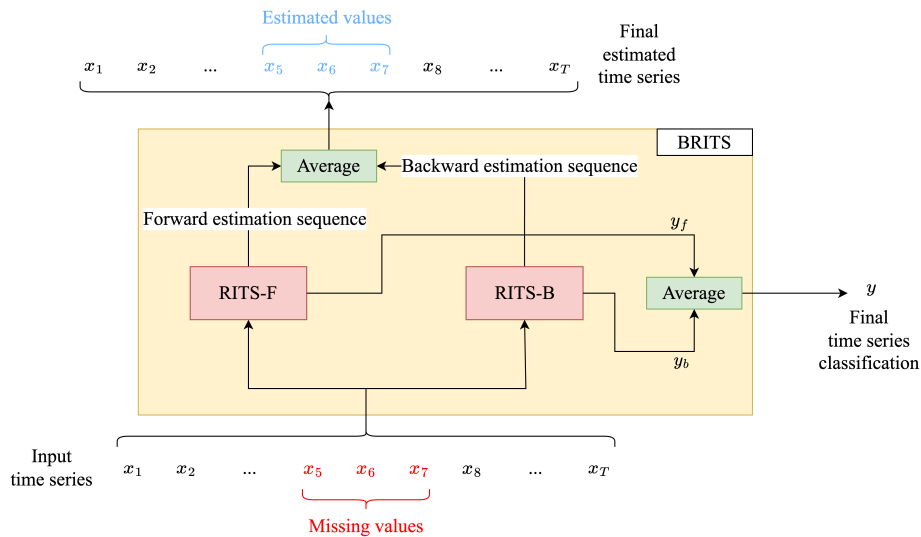


Figure 3: BRITS architecture.

4 Study area and data construction

This section describes the study area and provides full details on how the used dataset was built and processed.

4.1 Study area

Andalusia is the second-largest, most populous, and southernmost autonomous community in Peninsular Spain (Figure 4). Andalusia is one of the most biodiverse and heterogeneous regions of Europe. It contains steep altitudinal gradients, and it has a wide variety of landscapes and climatic conditions which results in a vast variety of vegetation types that hold the greatest diversity of plant and animal species in Europe. The long and dynamic history of human activities has also led to a complex landscape configuration with frequent mosaics of small patches of different types of natural, semi-natural land covers and human land uses. Hence, Andalusia offers an ideal field laboratory to test the creation of detailed and fine scale LULC maps containing the abundance of each LULC class per pixel to monitor the socioeconomic and environmental dynamics in complex landscapes using DL and multispectral time series of satellite imagery.



Figure 4: Study area: Andalusia, Spain.

4.2 Andalusia-MSMTU dataset construction

To build Andalusia MultiSpectral, MultiTemporal Unmixing dataset, named Andalusia-MSMTU, several sources were utilized: MODIS, GEE [32], REDIAM's environmental information [33] and SIPNA [12]. Herein, three different processes were used to create the dataset, (1) MODIS multispectral time series extraction, (2) ancillary data extraction and LULC abundances annotations.

4.2.1 MODIS pixel time series extraction

The time series data were extracted from Terra and Aqua satellites using MODIS sensor at 460m spatial resolution and at monthly temporal resolution. As LULC changes during one year are very limited in a 460m pixel, we assume that the LULC abundances are representative of the full year.

Spatio-temporal filtering was applied using MODIS 'Quality Assessment' (QA) flags and the "State QA" flags. Moreover, as the process of Terra and Aqua data filtering generates many missing values, to further reduce the amount of noise in the data, two solutions were employed: (1) the 8-days time series data were transformed into monthly

composites by computing the monthly mean from the individual observations, then (2) the monthly data from the Terra and Aqua satellites were combined to generate a merged Terra+Aqua monthly dataset. All this process was performed in Google Earth Engine (GEE) [32] and inspired by [34].

4.2.2 Ancillary data extraction for each MODIS pixel

In addition to the MODIS data, for every pixel we included geographic, topographic, and climatic ancillary information. Pixel longitude and latitude were directly extracted from MODIS metadata. Pixel altitude was obtained by averaging a 30m/pixel digital elevation model [35] to 460m/pixel. MODIS pixel slopes were calculated using GEE slope calculation algorithm on the same 30m elevation model and averaged to 460m resolution. Finally, climatic data were downloaded from REDIAM’s environmental information [33], including potential evapotranspiration, precipitation, mean annual temperature, mean of the maximum temperatures, and mean of the minimum temperatures.

4.2.3 Pixels’ LULC abundances annotation from SIPNA

To annotate each MODIS pixel with the abundance of each LULC class, the official LULC map of Andalusia for the year 2013 (SIPNA) [12] was used. Given the coarse resolution of MODIS pixels we only considered level 1 (four classes) and an adapted version of level 2 (ten classes) of the classification hierarchy of SIPNA (Figure 5).

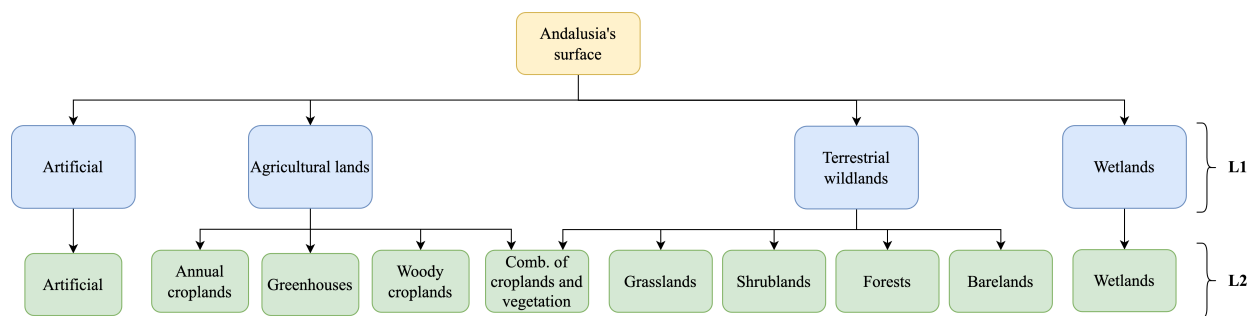


Figure 5: Hierarchical structure of the SIPNA-based LULC classes. The blue boxes represent the level 1 (L1) classes. The green boxes represents the Level 2 (L2) classes.

Given that SIPNA provides information at sub-pixel level, we calculated the exact abundances of all the LULC classes existing in each MODIS 460m resolution pixel, as illustrated in Figure 6, using QGIS software [36] as follows: the SIPNA polygons were first converted to raster format providing a LULC map at 10m resolution. The rasterized map was then converted to match the spatial resolution of MODIS, resulting in the class proportions for each pixel of Andalusia. Finally, the MODIS pixels abundances annotations were coupled with their corresponding time series and ancillary data to obtain the Andalusia-MSMTU dataset. In Figure 7 it is showed an example of the calculation of class abundances for a given pixel. An illustrative example of the distribution of abundances of LULC classes in level 1 of the classification hierarchy over the Andalusia territory is displayed in Figure 8, being "agricultural lands" and "terrestrial lands" the classes that dominate the Andalusian territory. Andalusia-MSMTU dataset [37] is available in a public data repository hosted by Zenodo at: <https://zenodo.org/record/7752348#.ZBmkkezMLdo>

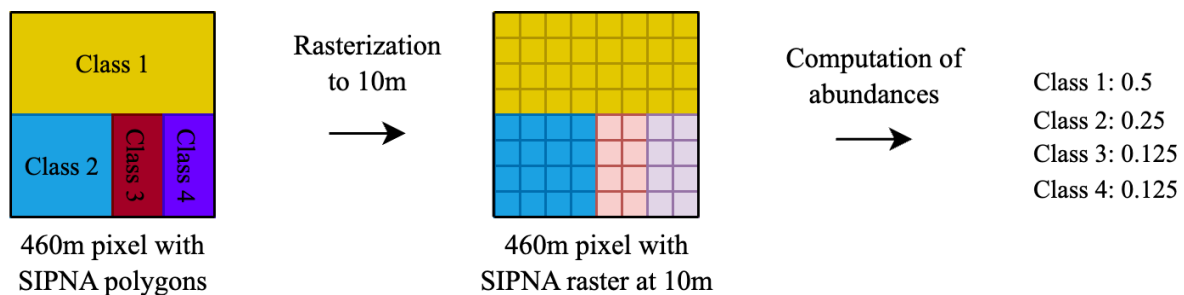


Figure 6: The used scheme for extracting class abundances in every MODIS pixel of Andalusia. The original SIPNA polygons were rasterized to 10m × 10m then the LULC abundances were computed for each 460m × 460m pixel.

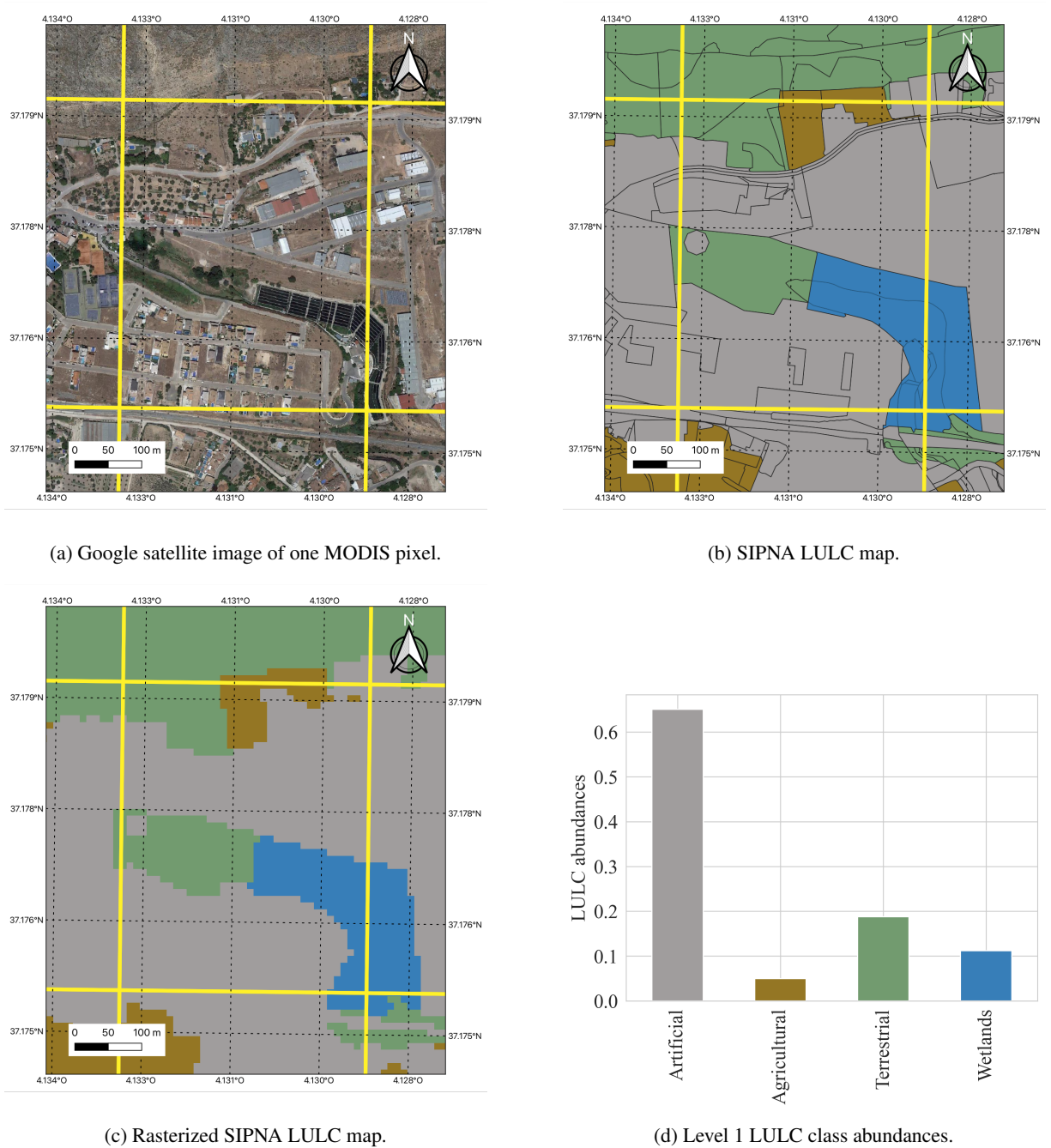


Figure 7: Example of how class abundances are obtained for each MODIS pixel. (a) shows the satellite image of the Google Satellite corresponding to one MODIS pixel. (b) shows the annotated SIPNA polygons. (c) the rasterized LULC map at 10m resolution. (d) the obtained abundance of level 1 classes for that MODIS pixel.

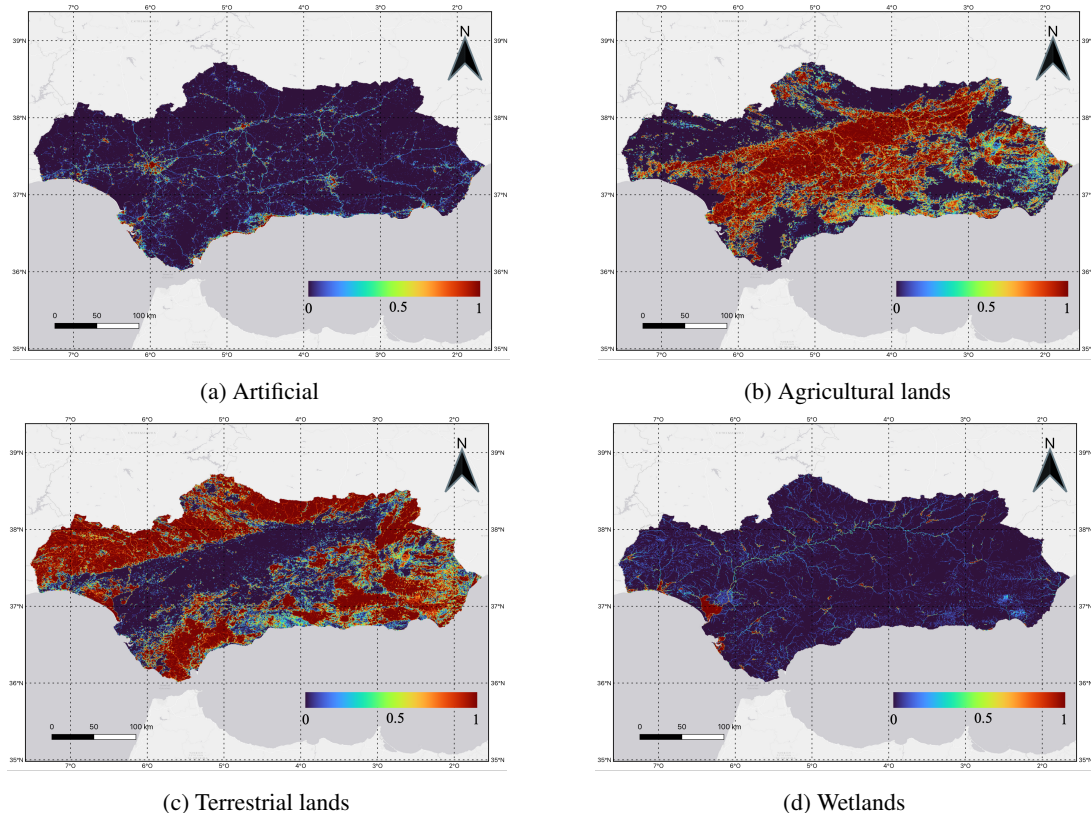


Figure 8: Gradient map of abundances from Andalusia 460m pixels for each LULC class in level 1 of SIPNA: (a) Artificial, (b) Agricultural lands, (c) Terrestrial lands, and (d) Wetlands. Blue pixels represent low abundance and red pixels represent high abundance.

5 Methodology

Formally, we have a set of n multispectral time series pixels $\{X_1, X_2, \dots, X_n\}$ with their corresponding class abundances $\{y_1, y_2, \dots, y_n\}$ where $y_i \in S^C, i \in [1, n]$. S^C is the sample space of class abundances commonly referred to as the simplex [38]. In our case C is equal to 4 and 10 for level 1 and 2 of the hierarchy, respectively.

To enhance class abundance estimation further, in addition to using the multispectral multitemporal data we also include ancillary information from two types:

- **Geo-topographic data:** Geographical coordinates (longitude and latitude), altitude and slope. Incorporating geographic coordinates can help the model understand the spatial distribution of land cover types, which can be valuable in guiding the spectral unmixing process and making it more contextually accurate. Similarly, adding topographic data (altitude and slope) provides useful information that complements the spectral characteristics of a pixel. In fact, terrain slope is known to influence surface reflectance, so incorporating it into the model can allow slope-related changes in reflectance to be taken into account, making its predictions more robust.
- **Climatic data:** Precipitation, potential evapotranspiration, mean temperature, maximum temperature and minimum temperature. Some land cover classes, such as agricultural lands, forests, and wetlands, respond differently to variations in climate. By using climatic variables, the DL model can distinguish between these climate-dependent classes more effectively.

Below, we describe the architecture of the used model and the evaluation metrics.

5.1 Model architecture

Our approach to estimate the class abundances using multispectral multitemporal data and ancillary information for each mixed pixel is depicted in Figure 9. The proposed approach includes three components:

1. Spectro-temporal feature extraction: We use BRITS model [31] to extract the spectro-temporal patterns in presence of missing values from our dataset.
2. Ancillary data feature extraction: To incorporate ancillary information, we process the external information using a linear layer with ReLU non-linearity.
3. Concatenation and features combination: The output features of part (1) and (2) are concatenated and processed by a final dense layer that outputs C (the number of classes) scores.

The final dense layer generates an unbounded outputs \mathbf{o} where $\mathbf{o} \in \mathbb{R}^C$ with C being the number of classes. Following the work of [39], we applied the softmax transformation to obtain the final abundances predictions $\mathbf{a} \in S^C$:

$$a_j = \frac{e^{o_j}}{\sum_{c=1}^C e^{o_c}} \quad (3)$$

where a_j denotes the abundance prediction for the j th class, o_j denotes the final layer's output associated with the j th class.

Finally, the NN is optimized by minimizing the mean-square error (MSE) between the abundances predictions and the reference abundances:

$$MSE = \frac{\sum_{i=1}^N \sum_{c=1}^C (r_{ic} - a_{ic})^2}{N} \quad (4)$$

where r_{ic} and a_{ic} are the reference abundance and the predicted abundance, respectively, for the c th class in the i th sample, and N is the number of training samples.

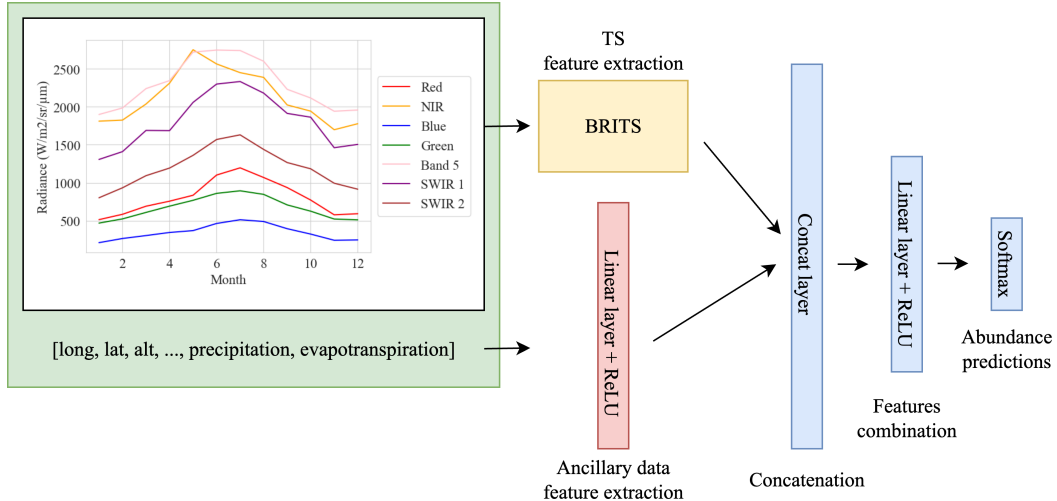


Figure 9: Our proposed neural network. The green box denotes the input data for a given pixel, i.e., multispectral time series data + ancillary data. The yellow box denotes the BRITS model for multispectral time series feature extraction, the red box denotes the ancillary data feature extraction layer and the blue boxes denote the final layers for features combination and softmax transformation of neural network's output.

5.2 Evaluation criteria

To assess the effectiveness of the proposed unmixing model, four regression metrics are examined:

- Pearson's Correlation Coefficient (CC):

$$CC = \frac{\sum_{i=1}^N (r_i - \bar{r})(a_i - \bar{a})}{\sqrt{\sum_{i=1}^N (r_i - \bar{r})^2 \sum_{i=1}^N (a_i - \bar{a})^2}} \quad (5)$$

- Root Mean Squared Error (RMSE):

$$RMSE = \sqrt{\frac{1}{n} \sum_{i=1}^N (r_i - a_i)^2} \quad (6)$$

- Relative Root Mean Squared Error (RRMSE):

$$RRMSE = \sqrt{\frac{\sum_{i=1}^N (r_i - a_i)^2}{\sum_{i=1}^N (r_i)^2}} \quad (7)$$

- Mean Absolute Error (MAE):

$$MAE = \frac{1}{n} \sum_{i=1}^N |r_i - a_i| \quad (8)$$

where r_i is the reference abundance, a_i the predicted abundance, and \bar{r} and \bar{a} are the mean of both variables. Finally, we also considered F1-score (Formula 9) to evaluate how good is the model in predicting the majoritarian class in each mixed pixel.

$$F1 = \frac{2 * TP}{2 * TP + FP + FN} \quad (9)$$

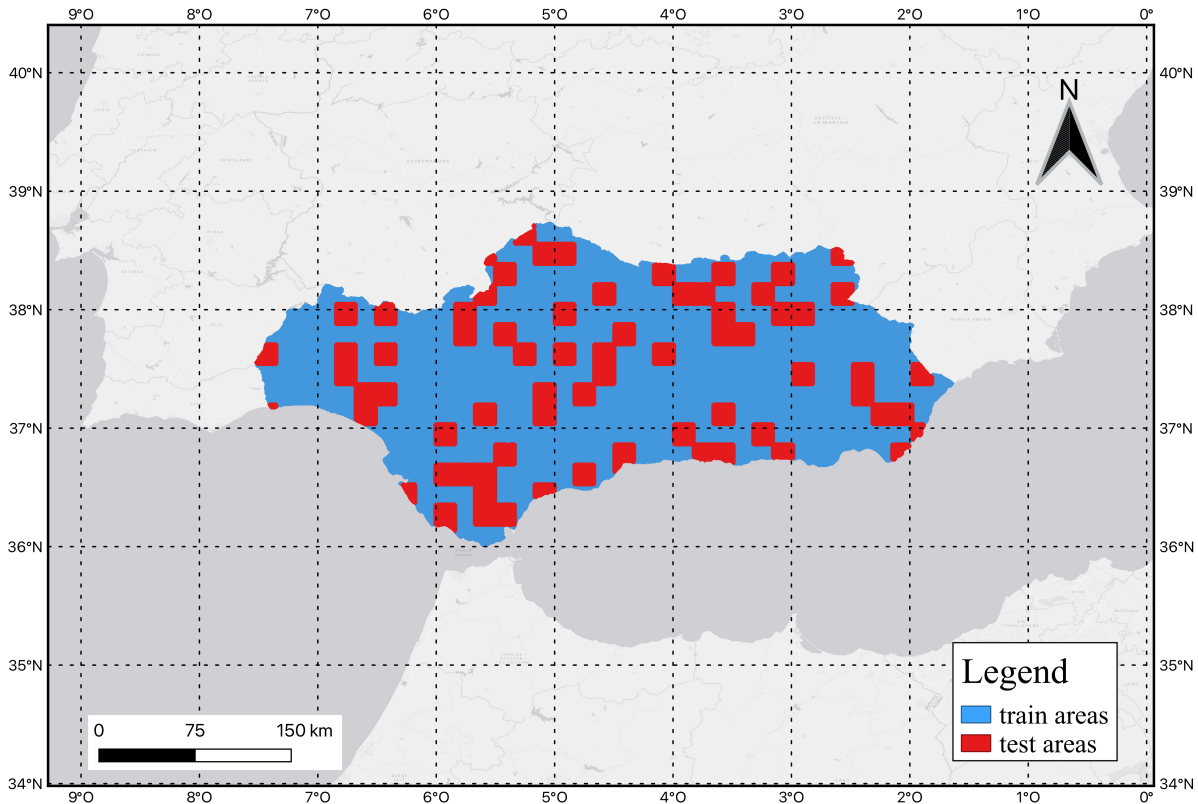


Figure 10: Train (blue) and test (red) areas.

5.3 Experimental design

To analyse the effect of introducing ancillary data and using different levels of the LULC legend on the performance of our DL approach for spectro-temporal unmixing, we considered different input data combinations, that is: using (1) only the multispectral time series data, (2) time series plus geo-topographic ancillary data, (3) time series plus climatic ancillary data, and (4) time series plus geo-topographic and climatic ancillary data.

In order to avoid spatial autocorrelation of neighbouring pixels we used a block train test splitting [40, 41]. Firstly, we divided the entire Andalusian territory in areas of equal size using blocks of 18x15 kilometers, which means that each block contains 1250 460m pixels approximately. Subsequently, 80% of the pixel blocks were assigned randomly to the training set, with the remaining 20% allocated to the test set. Figure 10 illustrates the areas of pixels designated for the training and testing sets. The source code to run these experiments will be available after acceptance at <https://github.com/jrodriguezortega/MSMTU>.

Implementation details: Our models undergo training using the Adam optimizer [42] for a total of 200 epochs with a batch size of 2048. We initialize the learning rate at 0.003 and progressively reduce it via the cosine learning rate decay scheduler. All experiments were conducted utilizing the PyTorch deep learning framework [43].

TimeSpec4LULC [34] pre-training: TimeSpec4LULC is an open-source dataset comprising multispectral time series data for 29 LULC classes, designed for training machine learning models. This dataset is constructed using the seven spectral bands from MODIS sensors, providing data at a 460m resolution, spanning the time period from 2000 to 2021. We found that pre-training BRITS model on TimeSpec4LULC dataset and fine-tuning it on Andalusia-MSMTU provides better results than training it from scratch, mainly because of the similarity between both datasets.

6 Experimental results

This section provides the experimental results of the proposed model at SIPNA level 1 and level 2.

6.1 SIPNA level 1

We evaluated the proposed model in Section 5 on different combinations of spectro-temporal data and ancillary data. In particular, we considered these combinations: (spectro-temporal data), (spectro-temporal data + geo-topographic data), (spectro-temporal data + climatic data) and (spectro-temporal data + geo-topographic and climatic data). The results of this four data combinations in terms of the average MAE, RMSE, RRMSE, CC, and F1-score, across the four classes of level 1 are provided in Table 2. As it can be seen, in general, including ancillary information always improves the spectral unmixing performance with respect to the baseline model (using multispectral time series only). The highest performance is achieved when including both, geo-topographic and climatic data together with the multispectral time series showing the lowest MAE, RMSE and RRMSE, with 0.55%, 0.63% and 2.07% of improvement respectively and highest CC and F1-score with 0.0153 and 0.0101 of improvement respectively, with respect to the baseline model.

Table 2: Performance comparison in terms of average Mean Absolute Error (MAE), Root Mean Squared Error (RMSE), Relative Root Mean Squared Error (RRMSE), Correlation Coefficient (CC) and F1-score of the spectral unmixing for SIPNA level 1 classes. "Ancillary" column indicates the included ancillary information in each evaluation.

Ancillary data added	MAE (%)	RMSE (%)	RRMSE (%)	CC	F1-score
None	6.70%	12.28%	42.40%	0.8570	0.8140
Geo-topographic	6.21%	11.80%	40.84%	0.8691	0.8195
Climatic	6.55%	12.24%	42.34%	0.8582	0.8107
Geo-topographic + climatic	6.15%	11.65%	40.34%	0.8723	0.8241

A further analysis of the five metrics for each class is depicted in Figure 11. In general, including the geo-topographic and climatic information improves the abundance predictions of all the classes of level 1. The "terrestrial lands" and "agricultural lands" achieve better performance in terms of CC, F1-score and RRMSE. However, the classes that benefit the most from adding the ancillary data are "artificial" and "wetlands" since the relative improvement is greater in these classes.

It is worth noting that the RMSE and MAE metrics are not fair for comparisons between classes as they do not take into account the range of abundance values within each class. The most appropriate metric for these comparisons in this case is the RRMSE.

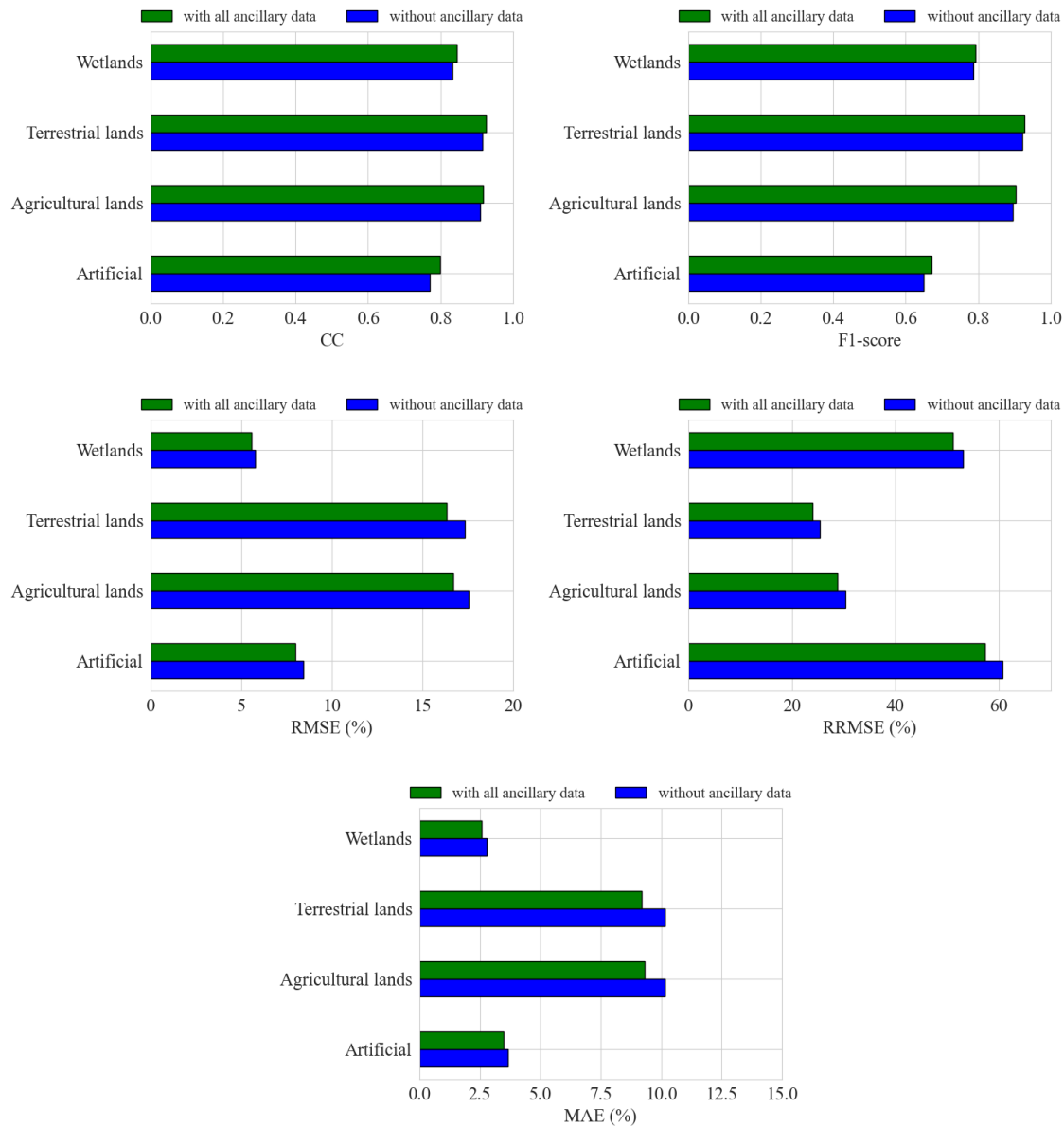


Figure 11: Test results for the four SIPNA level 1 classes obtained by including all ancillary information (green) and without ancillary information (blue): CC values (top left), F1-score values (top right), RMSE values (middle left), RRMSE values (middle right), and MAE values (bottom).

To better illustrate the reasons behind these differences in performance between observed and predicted abundances in each of the four LULC classes, Figure 12 shows a density scatter plot for each class. The scatter plots of "artificial" and "wetlands" pixels showed a less aligned distribution along the 1:1 straight line than terrestrial and agricultural lands. In artificial and wetlands plots, most points are concentrated in the lowest abundances, while in terrestrial and agricultural lands plots tend to concentrate in both the extremes of the abundance gradient but also along the 1:1 line. This proves that the model works reasonably good for both abundant (terrestrial and agricultural lands) and scarce (artificial and wetlands) classes.

Finally, Figure 13 shows the results achieved by the best model on three test areas (top row) with their corresponding RMSE (middle row) and RRMSE (bottom row) per pixel maps. As we can observe, most of the pixels are in blue tones, which indicates a low RMSE and RRMSE and a great LULC abundances predictions. A reduced number of pixels with red tones in the RRMSE maps indicates an important prediction error relative to the scale of the reference abundance.

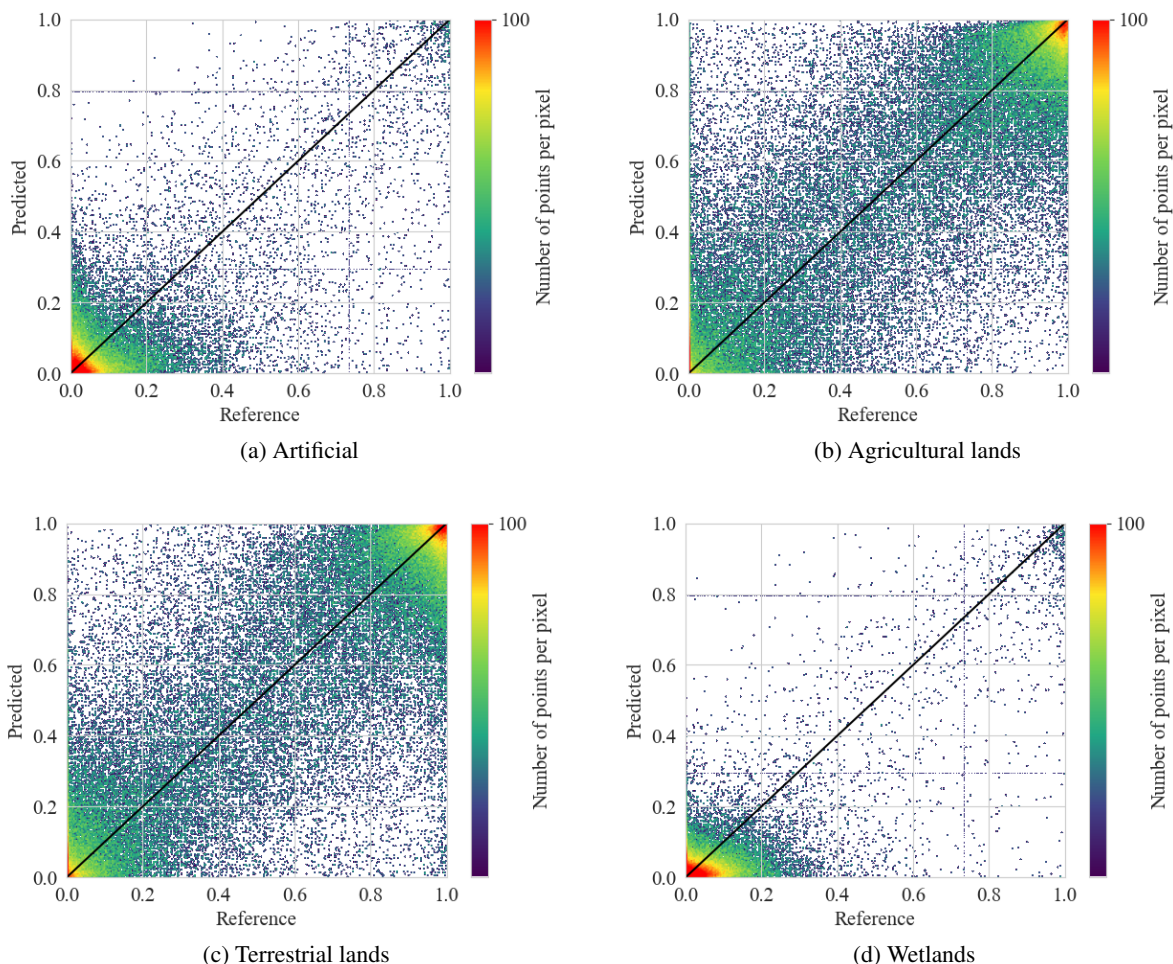


Figure 12: Density scatter plots of every level 1 class abundances (predicted vs reference) for the best model (including all ancillary data). (a) Artificial, (b) Agricultural lands, (c) Terrestrial lands, and (d) Wetlands.

These pixels mainly correspond to small rural areas with a large diversity of urban, crop and even forest areas, which makes the task of correctly predicting each and every LULC class abundances very difficult.

6.2 SIPNA level 2

Similarly, we evaluated the proposed model on these input combinations: (spectro-temporal data), (spectro-temporal data + geo-topographic data), (spectro-temporal data + climatic data) and (spectro-temporal data + geo-topographic and climatic data) considering SIPNA level 2.

Again, including ancillary information improves the spectral unmixing task even in a much more difficult spectral unmixing setting (Table 3). Compared to the baseline, the best performing model (including all the ancillary data) decreases the MAE, RMSE and RRMSE by 0.31%, 0.28% and 1.68%, respectively and increases CC and F1-score by 0.0160 and 0.0188, respectively.

In the same way as in level 1, Figure 14 shows a comparison between the baseline model and the model including geo-topographic and climatic data for every class in each of the five metrics used for evaluation. In general, adding ancillary information improves the abundances predictions of all the classes. The best performance is achieved in "woody crops" and "annual crops" classes in terms of CC, F1-score and RRMSE. Besides, adding the ancillary information to the model achieves a greater improvement for the classes with the worst results like "combinations of croplands and vegetation", "barelands" and "artificial".

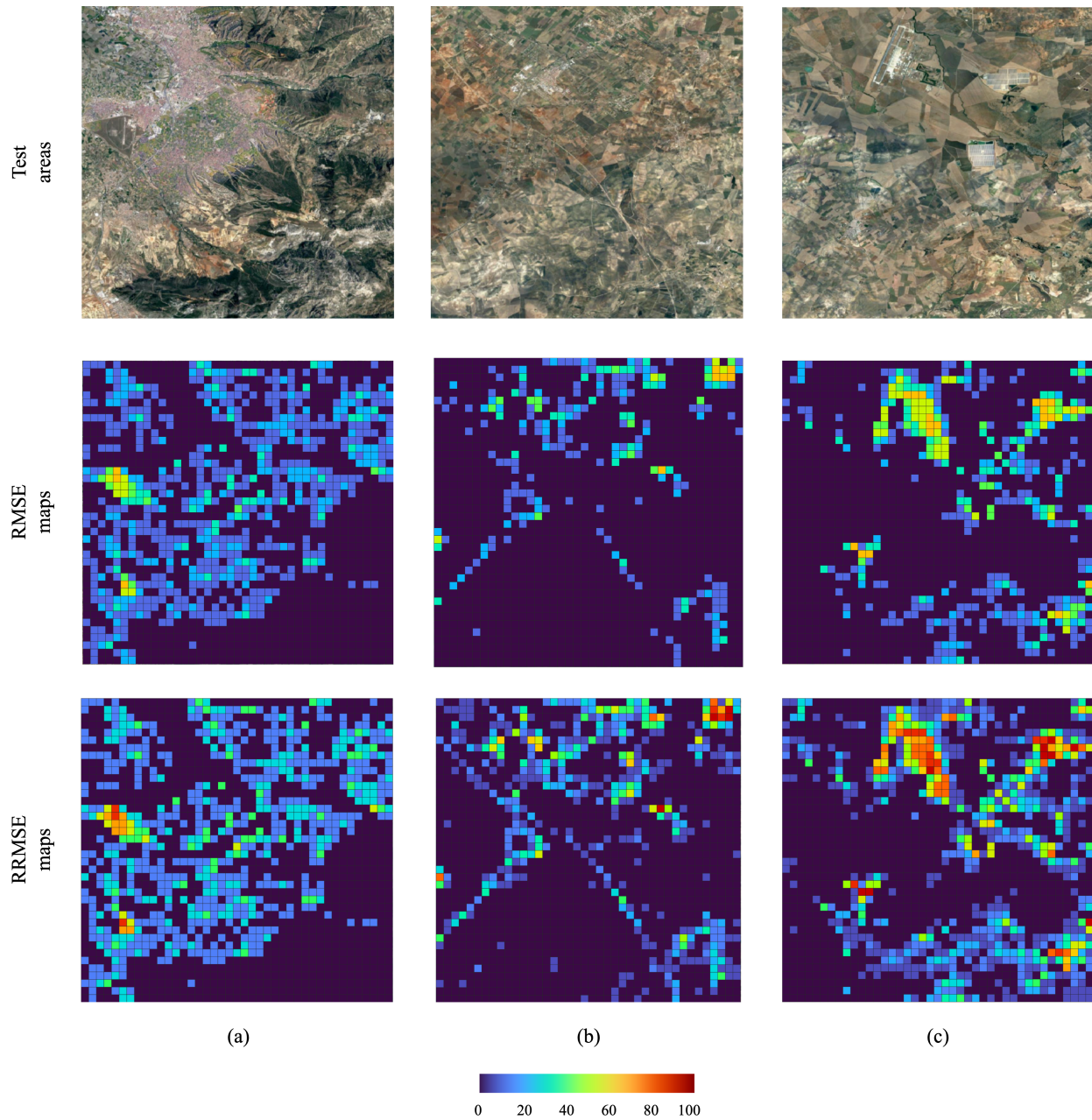


Figure 13: Three test areas (top row) with their corresponding RMSE (middle row) and RRMSE (bottom row) per pixel maps in level 1. (a) Granada, Granada, (b) La Carlota, Córdoba, (c) El Coronil, Sevilla.

Table 3: Comparison in terms of average MAE, RMSE, RRMSE, CC and F1-score of the spectral unmixing for SIPNA level 2 classes. "Ancillary" column indicates the included ancillary information in each evaluation.

Ancillary data added	MAE (%)	RMSE (%)	RRMSE (%)	CC	F1-score
None	5.88%	11.54%	59.11%	0.7504	0.6216
Geo-topographic	5.60%	11.31%	57.92%	0.7635	0.6396
Climatic	5.73%	11.47%	58.57%	0.7566	0.6317
Geo-topographic + climatic	5.57%	11.26%	57.43%	0.7664	0.6404

Looking at the density scatter plot for each level 2 class in Figure 15, we see that the correlation between the reference and the predicted abundances is generally good, except for "combinations of croplands and vegetation" and "barelands"

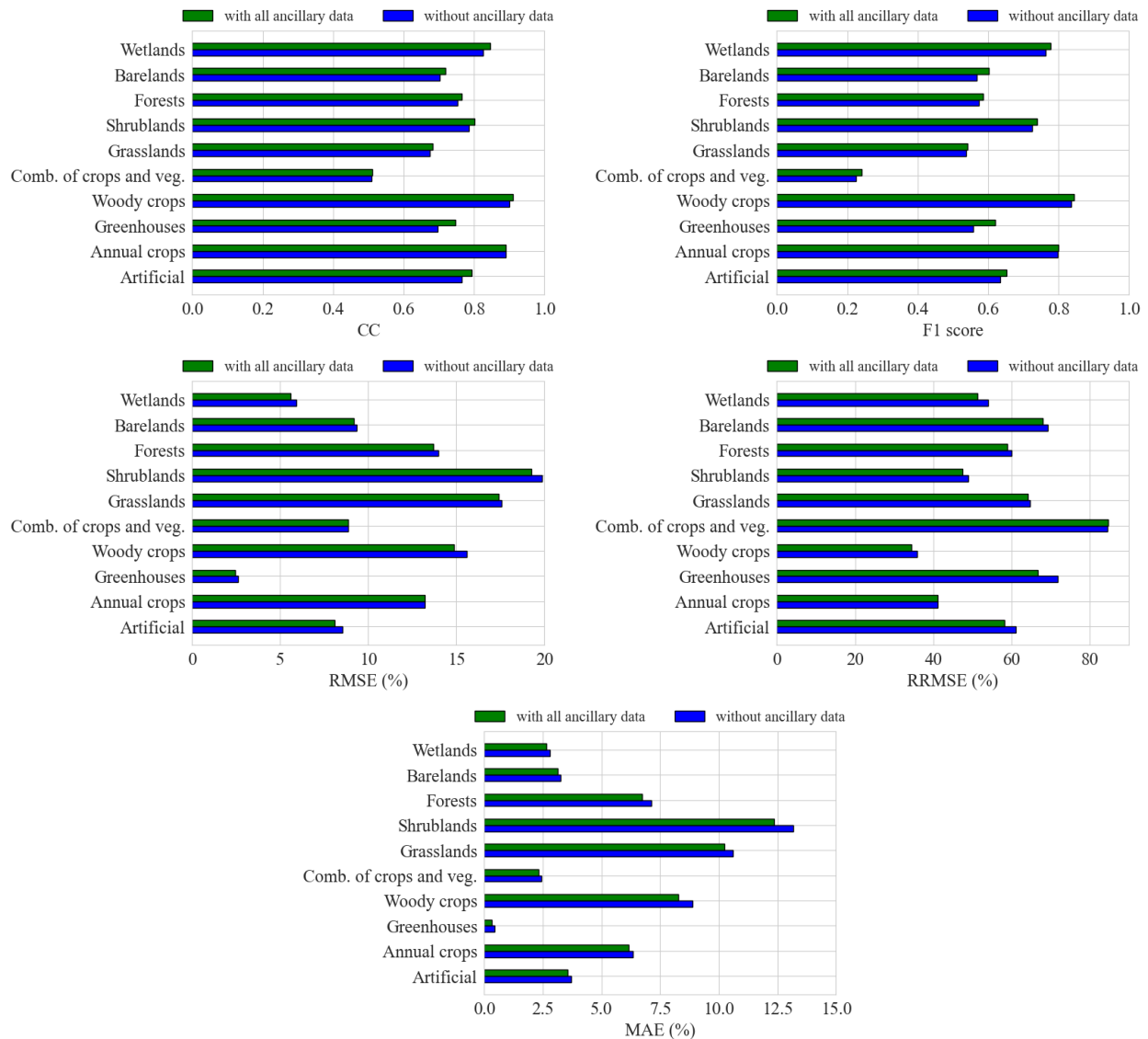


Figure 14: Test results for the ten SIPNA level 2 classes obtained by including all ancillary information (green) and without ancillary information (blue): CC values (top left), F1-score values (top right), RMSE values (middle left), RRMSE values (middle right), and MAE values (bottom).

classes since they show a large dispersion. It is worth emphasizing the strong performance of the model for the class "greenhouses". Despite of having so few representation of middle range values of abundance in the pixels of Andalusia, the correlation in this class between the reference and predicted abundances is similar to the classes with a good representation. We argue that the reason for that could be due to their very high albedo, i.e., high reflectance in all bands. Finally, the worst performance metrics were obtained for "combinations of croplands and vegetation" class, which may be due to the mixed-nature of this class definition itself. By combining crop and vegetation this class is a mixture of some of the other classes and hence it is complicated for the model to predict the correct abundances.

Lastly, Figure 16 shows the results achieved by the best model on three test areas (top row) with their corresponding RMSE (middle row) and RRMSE (bottom row) per pixel maps. In general, most pixels are in dark blue tones (low error) in the RMSE maps, which at first glance may seem better than the results achieved for level 1. However, when looking at the RRMSE maps we can notice a slightly higher number of pixels with red tones than in the level 1 RRMSE maps, located mainly in small rural towns. This means that although the error at SIPNA level 1 is lower in absolute terms, when it is relativized by the scale of the reference abundances it becomes higher than in level 1, indicating only moderate results compared to the good results obtained at level 1. For this reason, it is recommended to evaluate not only the RMSE but also the RRMSE to get better conclusions.

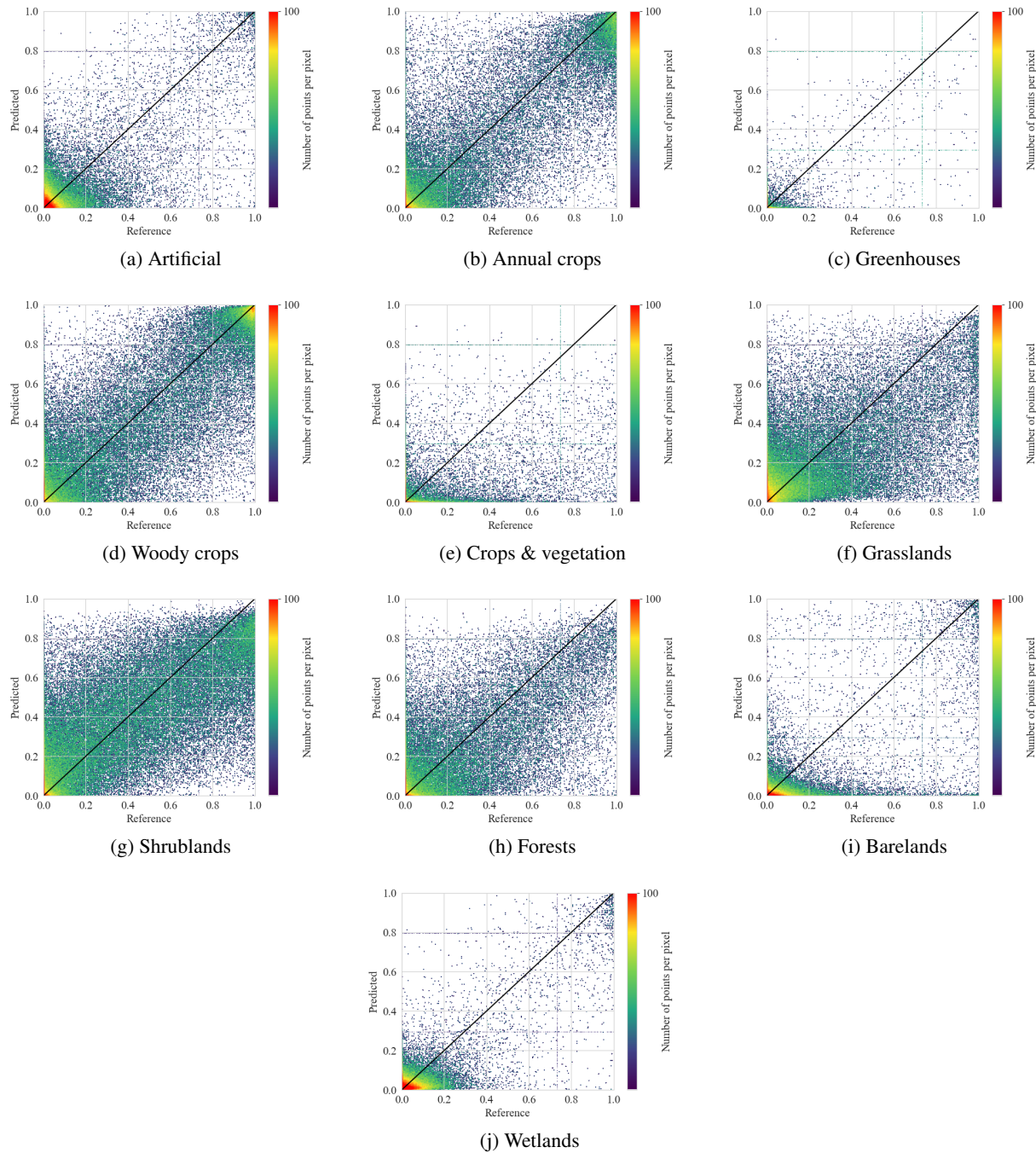


Figure 15: Density scatter plots of every level 2 class abundance (predicted vs reference) for the best model (including all ancillary data). (a) Artificial, (b) Annual croplands, (c) Greenhouses, (d) Woody croplands, (e) Combinations of croplands and vegetation , (f) Grasslands and grasslands with trees, (g) Shrublands and shrublands with trees, (h) Forests, (i) Barelands, and (j) Wetlands.

7 Discussion

Spectral unmixing of LULC classes is a challenging problem commonly addressed by physical models with the need for endmember extraction [3, 4]. DL methods represent a great solution as a BSU based approach to eliminate the need for endmember extraction. Most previous works focus on hyperspectral or multispectral data and do not exploit temporal information to estimate the abundance of mixed pixels. Obtaining multispectral time series of large territories can be prohibitive due to the cost and time required to acquire them [44, 45]. In addition, no previous work has explored

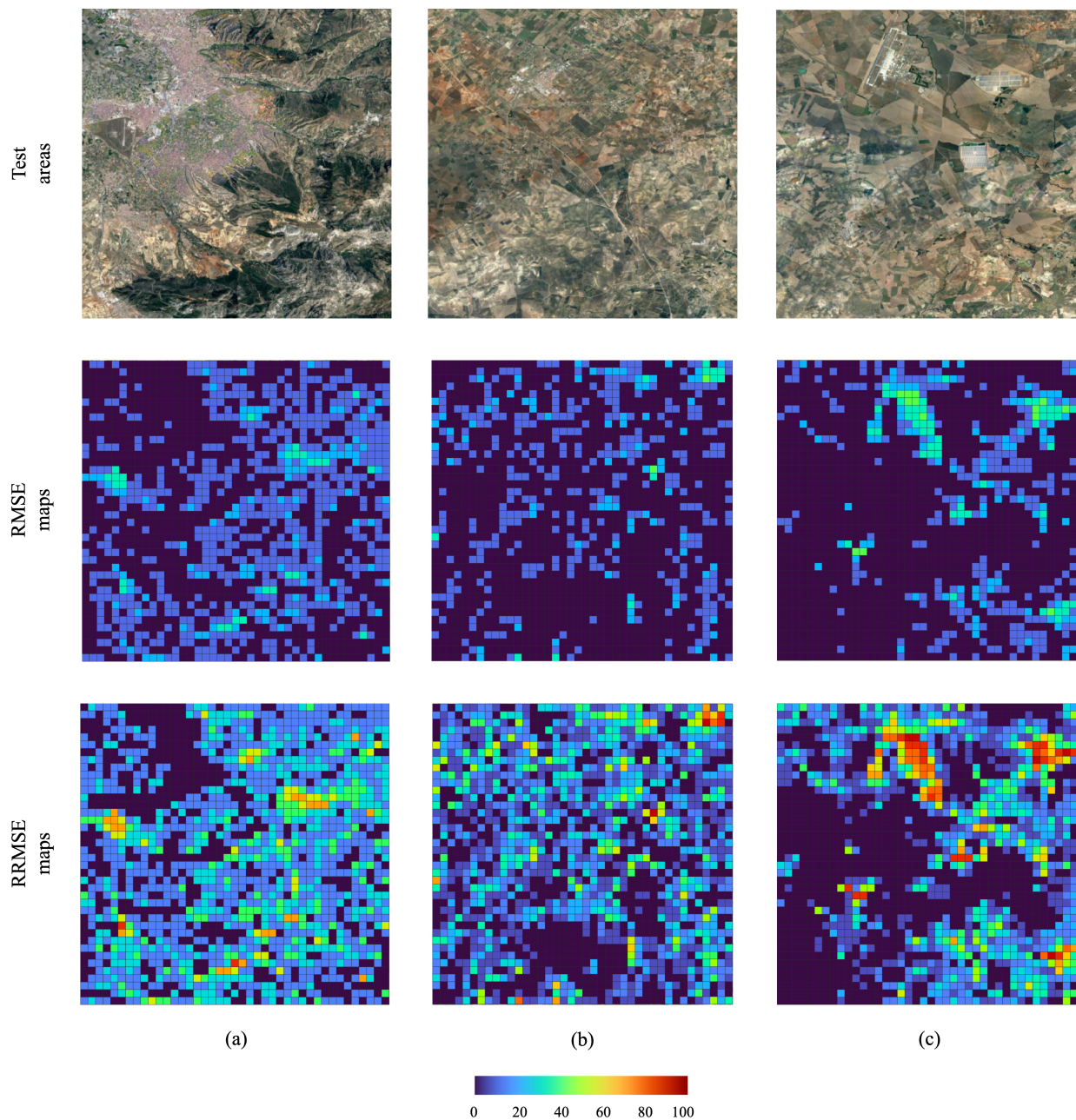


Figure 16: Three test areas (top row) with their corresponding RMSE (middle row) and RRMSE (bottom row) per pixel maps in level 2. (a) Granada, Granada, (b) La Carlota, Córdoba, (c) El Coronil, Sevilla.

the possibility of adding ancillary data to enhance the spectral unmixing results, which are used successfully in other computer vision tasks [9, 10, 11].

In this work, we tried to solve the mentioned constraints of previous works by: (1) developing Andalusia-MSMTU, a multispectral time series dataset of mixed pixels labeled with LULC class abundances at two classification levels and making it publicly available so other researchers can develop new approaches in the field of spectral unmixing, and (2) proposing and analysing DL-based approaches for BSU.

Our results showed that our DL-based method achieved good results for spectral unmixing of LULC classes by using multispectral data. Besides, by including ancillary information the model improved in terms of every metric used for evaluation, showing that adding external data is an interesting avenue to explore in spectral unmixing problems.

Finally, one significant limitation still exists in our work. Although DL models have shown great performance in mapping complex input-output relationships and have demonstrated promising results for BSU of LULC classes, they lack physical interpretability. This means that it is difficult to understand how the model arrived at its decision, and it may not be clear why certain input features were given more weight than others [46]. In the context of spectral unmixing, physical interpretation may be desirable [47] because it allows us to understand the underlying physical processes that govern the interaction of electromagnetic radiation with land surface materials.

8 Conclusions

In this work, we introduced and made publicly available Andalusia-MSMTU dataset, a new DL-ready dataset to explore BSU approaches on multispectral time series data. Furthermore, we introduced ancillary information to improve the spectral unmixing performance consisting on two geographic, two topographic and five climatic variables. Our experiments show that the use of multispectral time series data for LULC abundance estimation achieves good results, which can be further improved by including ancillary information.

For future work, we would like to explore taking advantage of spatial autocorrelation between neighbouring pixels, which provides useful information for the spectral unmixing task [48], by arranging the MODIS pixels in images and using a Convolutional-LTSM network with a BRITS-like approach to deal with missing values. Moreover, given the recent availability of higher spatial resolution sensors like Sentinel-2, data fusion between MODIS long-term data and Sentinel-2 higher resolution data is another avenue to explore to improve spectral unmixing performance. Finally, since common DL-based models lack physical interpretation and it is sometimes important in the context of spectral unmixing, an effort to make DL-based methods physically aware is worthwhile.

Acknowledgment

This research was partially supported by the project “Thematic Center on Mountain Ecosystem & Remote sensing, Deep learning-AI e-Services University of Granada-Sierra Nevada” (LifeWatch-2019-10-UGR-01), which has been co-funded by the Ministry of Science and Innovation through the FEDER funds from the Spanish Pluriregional Operational Program 2014-2020 (POPE), LifeWatch-ERIC action line and by the TED project with reference TED2021-129690B-I00 funded by the Ministry of Science and Innovation.

References

- [1] Robert A Schowengerdt. *Remote sensing: models and methods for image processing*. Elsevier, 2006.
- [2] Xiangrong Zhang, Yujia Sun, Jingyan Zhang, Peng Wu, and Licheng Jiao. Hyperspectral unmixing via deep convolutional neural networks. *IEEE Geoscience and Remote Sensing Letters*, 15(11):1755–1759, 2018.
- [3] Nirmal Keshava and John F Mustard. Spectral unmixing. *IEEE signal processing magazine*, 19(1):44–57, 2002.
- [4] Jignesh S. Bhatt and M. V. Joshi. Deep learning in hyperspectral unmixing: A review. In *IGARSS 2020 - 2020 IEEE International Geoscience and Remote Sensing Symposium*, pages 2189–2192, 2020.
- [5] Qunming Wang, Xinyu Ding, Xiaohua Tong, and Peter M Atkinson. Spatio-temporal spectral unmixing of time-series images. *Remote Sensing of Environment*, 259:112407, 2021.
- [6] Burkni Palsson, Johannes R. Sveinsson, and Magnus O. Ulfarsson. Blind hyperspectral unmixing using autoencoders: A critical comparison. *IEEE Journal of Selected Topics in Applied Earth Observations and Remote Sensing*, 15:1340–1372, 2022.
- [7] Preetam Ghosh, Swalpa Kumar Roy, Bikram Koirala, Behnood Rasti, and Paul Scheunders. Hyperspectral unmixing using transformer network. *IEEE Transactions on Geoscience and Remote Sensing*, 60:1–16, 2022.
- [8] John F Mustard, Lin Li, and Guoqi He. Nonlinear spectral mixture modeling of lunar multispectral data: Implications for lateral transport. *Journal of Geophysical Research: Planets*, 103(E8):19419–19425, 1998.
- [9] Thomas Berg, Jiongxin Liu, Seung Woo Lee, Michelle L Alexander, David W Jacobs, and Peter N Belhumeur. Birdsnap: Large-scale fine-grained visual categorization of birds. In *Proceedings of the IEEE Conference on Computer Vision and Pattern Recognition*, pages 2011–2018, 2014.
- [10] Jeffrey S Ellen, Casey A Graff, and Mark D Ohman. Improving plankton image classification using context metadata. *Limnology and Oceanography: Methods*, 17(8):439–461, 2019.
- [11] Gabriel Tseng, Hannah Kerner, and David Rolnick. Timl: Task-informed meta-learning for agriculture. *arXiv preprint arXiv:2202.02124*, 2022.

- [12] Siose andalusia. https://www.juntadeandalucia.es/medioambiente/portal/landing-page-%C3%ADndice/-/asset_publisher/zX2ouZa4r1Rf/content/sistema-de-informaci-c3-b3n-sobre-el-patrimonio-natural-de-andaluc-c3-ada-sipna-/20151,2023. [Online; Accessed 07-2023].
- [13] Giles M Foody. Relating the land-cover composition of mixed pixels to artificial neural network classification output. *Photogrammetric engineering and remote sensing*, 62(5):491–498, 1996.
- [14] PM Atkinson, MEJ Cutler, and H Lewis. Mapping sub-pixel proportional land cover with avhrr imagery. *International Journal of Remote Sensing*, 18(4):917–935, 1997.
- [15] Giorgio A Licciardi and Fabio Del Frate. Pixel unmixing in hyperspectral data by means of neural networks. *IEEE transactions on Geoscience and remote sensing*, 49(11):4163–4172, 2011.
- [16] Yang Yu, Yong Ma, Xiaoguang Mei, Fan Fan, Jun Huang, and Hao Li. Multi-stage convolutional autoencoder network for hyperspectral unmixing. *International Journal of Applied Earth Observation and Geoinformation*, 113:102981, 2022.
- [17] Ashish Vaswani, Noam Shazeer, Niki Parmar, Jakob Uszkoreit, Llion Jones, Aidan N Gomez, Łukasz Kaiser, and Illia Polosukhin. Attention is all you need. *Advances in neural information processing systems*, 30, 2017.
- [18] Chunyu Li, Rong Cai, and Junchuan Yu. An attention-based 3d convolutional autoencoder for few-shot hyperspectral unmixing and classification. *Remote Sensing*, 15(2):451, 2023.
- [19] Min Zhao, Longbin Yan, and Jie Chen. Lstm-dnn based autoencoder network for nonlinear hyperspectral image unmixing. *IEEE Journal of Selected Topics in Signal Processing*, 15(2):295–309, 2021.
- [20] Rob Heylen, Mario Parente, and Paul Gader. A review of nonlinear hyperspectral unmixing methods. *IEEE Journal of Selected Topics in Applied Earth Observations and Remote Sensing*, 7(6):1844–1868, 2014.
- [21] David B Lobell and Gregory P Asner. Cropland distributions from temporal unmixing of modis data. *Remote Sensing of Environment*, 93(3):412–422, 2004.
- [22] Raúl Zurita-Milla, Luis Gómez-Chova, Luis Guanter, Jan GPW Clevers, and Gustavo Camps-Valls. Multitemporal unmixing of medium-spatial-resolution satellite images: A case study using meris images for land-cover mapping. *IEEE Transactions on geoscience and remote sensing*, 49(11):4308–4317, 2011.
- [23] Fan Yang, Bunkei Matsushita, Takehiko Fukushima, and Wei Yang. Temporal mixture analysis for estimating impervious surface area from multi-temporal modis ndvi data in japan. *ISPRS journal of photogrammetry and remote sensing*, 72:90–98, 2012.
- [24] Chengbin Deng and Zhe Zhu. Continuous subpixel monitoring of urban impervious surface using landsat time series. *Remote Sensing of Environment*, 238:110929, 2020.
- [25] Eric L Bullock, Curtis E Woodcock, and Pontus Olofsson. Monitoring tropical forest degradation using spectral unmixing and landsat time series analysis. *Remote sensing of Environment*, 238:110968, 2020.
- [26] Qunming Wang, Xinyu Ding, Xiaohua Tong, and Peter M Atkinson. Real-time spatiotemporal spectral unmixing of modis images. *IEEE Transactions on Geoscience and Remote Sensing*, 60:1–16, 2021.
- [27] Feiyun Zhu. Hyperspectral unmixing: ground truth labeling, datasets, benchmark performances and survey. *arXiv preprint arXiv:1708.05125*, 2017.
- [28] David E Rumelhart, Geoffrey E Hinton, Ronald J Williams, et al. Learning internal representations by error propagation. Technical report, 1985.
- [29] Sepp Hochreiter and Jürgen Schmidhuber. Long short-term memory. *Neural computation*, 9(8):1735–1780, 1997.
- [30] Florian Gerber, Rogier de Jong, Michael E Schaepman, Gabriela Schaepman-Strub, and Reinhard Furrer. Predicting missing values in spatio-temporal remote sensing data. *IEEE Transactions on Geoscience and Remote Sensing*, 56(5):2841–2853, 2018.
- [31] Wei Cao, Dong Wang, Jian Li, Hao Zhou, Lei Li, and Yitan Li. Brits: Bidirectional recurrent imputation for time series. *Advances in neural information processing systems*, 31, 2018.
- [32] Noel Gorelick, Matt Hancher, Mike Dixon, Simon Ilyushchenko, David Thau, and Rebecca Moore. Google earth engine: Planetary-scale geospatial analysis for everyone. *Remote Sensing of Environment*, 2017.
- [33] Red de información ambiental de andalucía. <https://www.juntadeandalucia.es/medioambiente/portal/acceso-rediam,2023>. [Online; Accessed 07-2023].
- [34] Rohaifa Khaldi, Domingo Alcaraz-Segura, Emilio Guirado, Yassir Benhammou, Abdellatif El Afia, Francisco Herrera, and Siham Tabik. Timespec4lulc: a global multispectral time series database for training lulc mapping models with machine learning. *Earth System Science Data*, 14(3):1377–1411, 2022.

- [35] Tom G Farr, Paul A Rosen, Edward Caro, Robert Crippen, Riley Duren, Scott Hensley, Michael Kobrick, Mimi Paller, Ernesto Rodriguez, Ladislav Roth, et al. The shuttle radar topography mission. *Reviews of geophysics*, 45(2), 2007.
- [36] QGIS Development Team. *QGIS Geographic Information System*. QGIS Association, 2022.
- [37] José Rodríguez-Ortega, Rohaifa Khaldi, Domingo Alcaraz-Segura, and Siham Tabik. Andalusia-msmtu, March 2023. This research is part of the project "Thematic Center on Mountain Ecosystem and Remote sensing, Deep learning-AI e-Services University of Granada- Sierra Nevada" (LifeWatch-2019-10-UGR-01), which has been co-funded by the Ministry of Science and Innovation through the FEDER funds from the Spanish POPE 2014-2020, LifeWatch-ERIC action line.
- [38] John Aitchison. The statistical analysis of compositional data. *Journal of the Royal Statistical Society: Series B (Methodological)*, 44(2):139–160, 1982.
- [39] Stien Heremans, Johan AK Suykens, and Jos Van Orshoven. The effect of imposing ‘fractional abundance constraints’ onto the multilayer perceptron for sub-pixel land cover classification. *International Journal of Applied Earth Observation and Geoinformation*, 44:226–238, 2016.
- [40] David R Roberts, Volker Bahn, Simone Ciuti, Mark S Boyce, Jane Elith, Gurutzeta Guillera-Arroita, Severin Hauenstein, José J Lahoz-Monfort, Boris Schröder, Wilfried Thuiller, et al. Cross-validation strategies for data with temporal, spatial, hierarchical, or phylogenetic structure. *Ecography*, 40(8):913–929, 2017.
- [41] Leonardo Uieda. Verde: Processing and gridding spatial data using Green’s functions. *Journal of Open Source Software*, 3(29):957, 2018.
- [42] Diederik P Kingma and Jimmy Ba. Adam: A method for stochastic optimization. *arXiv preprint arXiv:1412.6980*, 2014.
- [43] Adam Paszke, Sam Gross, Francisco Massa, Adam Lerer, James Bradbury, Gregory Chanan, Trevor Killeen, Zeming Lin, Natalia Gimelshein, Luca Antiga, et al. Pytorch: An imperative style, high-performance deep learning library. *Advances in neural information processing systems*, 32, 2019.
- [44] Jizhen Cai, Hermine Chatoux, Clotilde Boust, and Alamin Mansouri. Extending the unmixing methods to multispectral images. In *Color and Imaging Conference*, volume 2021, pages 311–316. Society for Imaging Science and Technology, 2021.
- [45] Jakub Nalepa. Recent advances in multi-and hyperspectral image analysis. *Sensors*, 21(18):6002, 2021.
- [46] Alejandro Barredo Arrieta, Natalia Díaz-Rodríguez, Javier Del Ser, Adrien Bennetot, Siham Tabik, Alberto Barbado, Salvador García, Sergio Gil-López, Daniel Molina, Richard Benjamins, et al. Explainable artificial intelligence (xai): Concepts, taxonomies, opportunities and challenges toward responsible ai. *Information fusion*, 58:82–115, 2020.
- [47] Gustau Camps-Valls, Daniel H. Svendsen, Jordi Cortés-Andrés, Álvaro Mareno-Martínez, Adrián Pérez-Suay, Jose Adsuara, Irene Martín, Maria Piles, Jordi Muñoz-Marí, and Luca Martino. Physics-aware machine learning for geosciences and remote sensing. In *2021 IEEE International Geoscience and Remote Sensing Symposium IGARSS*, pages 2086–2089, 2021.
- [48] Chen Shi and Le Wang. Incorporating spatial information in spectral unmixing: A review. *Remote Sensing of Environment*, 149:70–87, 2014.